




Effects of Laser Power on the Microstructure Evolution and Mechanical Properties of Ti–6Al–4V Alloy Manufactured by Direct Energy Deposition

Yukyeong Lee¹ · Eun Seong Kim² · Sangeun Park¹ · Jeong Min Park² · Jae Bok Seol¹ · Hyoung Seop Kim^{2,3} · Taekyung Lee⁴ · Hyokyung Sung¹ · Jung Gi Kim¹ 

Received: 10 May 2021 / Accepted: 7 July 2021 / Published online: 1 October 2021
© The Korean Institute of Metals and Materials 2021

Abstract

Process optimization of additively manufactured Ti–6Al–4V alloy is an important aspect of the production of engineered, high-performance parts for the aerospace and medical industries. In this study, the microstructural evolution and mechanical properties of direct energy deposition processed Ti–6Al–4V alloy were investigated using different processing parameters. Experimental analyses revealed that the line energy density corresponding to the processing parameters of the direct energy deposition process influences the properties of additively manufactured Ti–6Al–4V alloy. First, an optimal line energy density limits the incidence and size of voids resulting from a lack of fusion to enhance both alloy strength and ductility. Second, an excessively high energy density induces the coarsening of prior-β grains to impair both alloy strength with the Hall–Petch relationship and alloy ductility due to the plastic deformation instability caused by the limited number of grains. These results indicate that both the extent of fusion and prior-β grain size affect the mechanical properties of additively manufactured Ti–6Al–4V alloy. Moreover, the results demonstrate the utility of the line energy density-based approach in determining the optimal processing parameters for realizing high-performance materials.

Keywords Additive Manufacturing · Titanium · Microstructure · Mechanical Property · Strengthening

1 Introduction

Ti-6Al-4 V(Ti64) alloy are one of the representative structural materials in the aerospace and biomedical industries because of their outstanding specific strength and

corrosion resistance [1–3]. Although this alloy has properties that make them well suited for application in industrial fields, the high chemical reactivity between titanium and steel tools significantly hampers the machining or manufacturing of complex-shaped parts [4]. To overcome the poor machinability of Ti64 alloy, additive manufacturing (AM) has emerged as a promising alternative manufacturing approach to traditional machining processes. Recently, laser-based AM has been developed to fabricate complex-shaped metallic parts combining high-energy laser beams and computerized design [5–7]. Among the various types of laser-based AM methods, the direct energy deposition (DED) method is particularly suited to fabricating large parts and repairing metallic components owing to its high degree of control and process capability [8, 9]. As a result of these advantages, DED methods have been developed to build and repair complex-shaped components, such as turbine blades and gears [10, 11].

Moreover, many researchers have investigated the mechanical properties and microstructural evolution of DED-processed materials [12–14]. One of the signature

✉ Hyokyung Sung
hksung@gnu.ac.kr

✉ Jung Gi Kim
junggi91@gnu.ac.kr

¹ Department of Materials Engineering and Convergence Technology (Center for K-Metals), Gyeongsang National University, Jinju 52828, Republic of Korea

² Department of Materials Science and Engineering, Pohang University of Science and Technology (POSTECH), Pohang 37673, Republic of Korea

³ Center for High Entropy Alloys, Pohang University of Science and Technology (POSTECH), Pohang 37673, Republic of Korea

⁴ School of Mechanical Engineering, Pusan National University, Busan 46241, Republic of Korea

characteristics of the laser-based process is its high energy, which induces a rapid melting–solidification cycle during DED [15, 16]. The rapid melting–solidification cycle allows the generation of non-equilibrium and metastable microstructures to produce additively manufactured products with unique properties. In the case of a Ti64 alloy, the rapid solidification rate of the laser-based AM process induces diffusionless and shear-type transformation, resulting in metastable α' martensite formation. Therefore, many studies have reported that laser-based AM-processed Ti64 alloy consist of fine α' martensite laths within columnar prior- β grains [17–19]. Because the solidification rate of laser-based AM processes depends on the processing parameters (e.g., laser power, scanning speed, powder feed rate) [20, 21], the effect of the processing parameters on the performance of additively manufactured alloy is an important aspect of process optimization.

Hence, several studies have investigated the relationship between the processing parameters and properties of laser-based AM-processed Ti64 alloy. Mahamood et al. reported that the microhardness of a Ti64 alloy decreases with decreasing laser scan speed since the molten pool under low scanning speed conditions is larger than under high scanning speed conditions [22]. Moreover, a relatively high scanning speed and powder feed rate during DED transform the Ti64 alloy microstructure from the Widmanstätten structure to α' martensite, resulting in an increase in microhardness [23]. Wu et al. revealed that the columnar prior- β grain width decreases with increasing laser scan speed, while the other processing parameters are fixed [24]. The evolution of these columnar prior- β grains is related to the molten pool size and lath morphologies in an additively manufactured Ti64 alloy; accordingly, Tan et al. revealed that β grain refinement is particularly effective in enhancing the strength of an electron beam-melted Ti64 alloy because the prior- β grain boundary absorbs more dislocations than the α/β phase

interface [25]. On the other hand, Lin et al. reported that the strengthening attributable to the presence of α lamellae with nano-dispersoids in an additively manufactured Ti64 alloy is more significant than that attributed to the presence of prior- β grains [26]. Moreover, Cheng et al. found that the strengthening of a laser metal deposition processed Ti64 alloy originates from its acicular α' martensitic microstructure [27]. These studies show that the strengthening mechanism of an additively manufactured Ti64 alloy depends on its complex microstructure; however, it remains unclear which is the dominant factor determining the strength of these materials.

In the present work, the effects of laser power on the microstructural evolution and mechanical properties of DED-processed Ti64 alloy was investigated. To evaluate the mechanical properties of additively manufactured Ti64 alloy, both microhardness measurements and tensile tests were conducted. The prior- β grain and acicular α' martensite lath of Ti64 alloy prepared under various processing conditions, were investigated by optical microscopy and scanning electron microscopy (SEM). To quantitatively discuss the relationship between the processing parameters and material properties, the line energy densities (LEDs) of the DED processes were calculated and the LEDs were correlated with the mechanical properties of the additively manufactured Ti64 alloy.

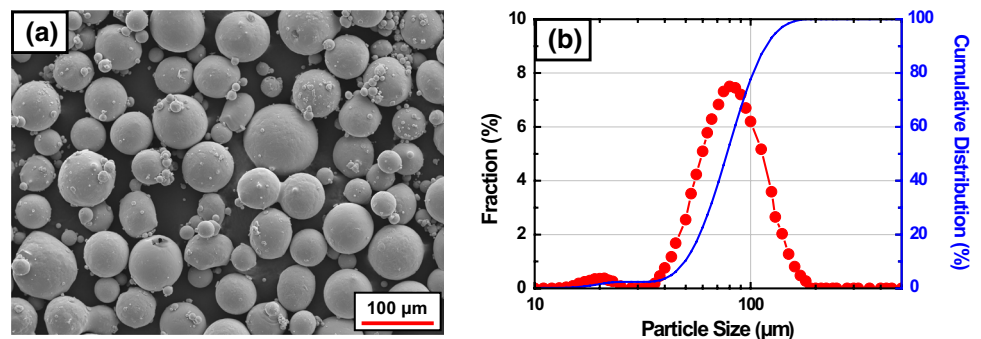
2 Experimental procedure

Table 1 presents the chemical composition of the Ti64 alloy investigated in this study. The spherical pre-alloyed Ti64 powder (MKmetal, Korea) shown in Fig. 1a was manufactured using gas atomization and sieving processes. The particle size distribution of the pre-alloyed Ti64 powder was assessed using a laser particle size analyzer (CILAS 1090

Table 1 Chemical composition of Ti64 pre-alloyed powder for DED

wt%	Ti	Al	V	Fe	O	N
Ti-6Al-4V	Bal	6.36	4.06	0.18	0.11	0.02

Fig. 1 **a** Initial morphology and **b** particle size distribution of the pre-alloyed Ti64 powder used for DED



LD Shape Analyzer, 3P Instruments, Germany), and Fig. 1b shows the particle size distribution of the Ti64 powder. The particle size distribution of the Ti64 alloy is equivalent to $d_{10} = 62.73 \mu\text{m}$, $d_{50} = 92.41 \mu\text{m}$, and $d_{90} = 144.70 \mu\text{m}$. Ti64 samples were manufactured by DED machine (MX-LAB, Insstek, Korea) under a powder feed rate and scan speed of 0.4 g/min and 850 mm/min respectively. To prepare samples, Ti64-1, Ti64-2, Ti64-3, and Ti64-4, with different LEDs, the laser power during DED was set to 160, 180, 200, and 220 W, respectively. The LED of each specimen was calculated as follows [28]:

$$\text{LED} = \frac{P}{v} \text{ (J/mm)}, \tag{1}$$

where P is the laser power (W) and v is the scan speed (mm/s). Based on Eq. (1), the LEDs of the specimens, Ti64-1, Ti64-2, Ti64-3, and Ti64-4 are 11.3, 12.7, 14.11, and 15.52 J/mm, respectively.

To neglect the effect of the scan strategy, the same scan strategy was applied in the fabrication of all the specimens; it followed a contour-filling-contour, zigzag pattern with a 90° rotation between layers, as described in Fig. 2. The closed-loop control of the DED process improves the uniformity of the samples and limits the incidence of local defects to optimize their mechanical properties [29]. To obtain tensile test samples, specimens with dimensions of 12 mm (width) × 18 mm (length) × 12 mm (height) were fabricated.

The mechanical properties of the Ti64 samples were evaluated by performing microhardness measurements and uniaxial tensile tests. The microhardness of the Ti64 samples was measured using a Vickers microhardness tester (HV-114, Mitutoyo, Japan) under an applied load of 0.5 kgf and a dwell time of 10 s. To assess the strength and ductility of the Ti64 samples, uniaxial tensile test specimens with gauge lengths of 1 mm were machined perpendicular to the

building direction. Uniaxial tensile tests were conducted using a universal testing machine (Micro UTM, R&B, Korea) at a quasi-static strain rate of $1 \times 10^{-3} \text{ s}^{-1}$. At least three tensile tests were conducted to reliably determine the mechanical properties of each Ti64 sample. The strain in the small tensile specimens was measured using a digital image correlation (DIC; ARAMIS 12 M adjustable, GOM Optics, Germany) technique and black and white speckle patterns. The detailed strain measurement method using DIC technique is explained in the authors’ previous work [30].

The mechanical properties of the Ti64 samples were correlated with their macro- and microstructures, analyzed by optical microscopy and electron backscatter diffraction (EBSD), respectively. To investigate the prior-β grain boundary morphology of the Ti64 specimens, samples—mechanically polished and etched using Kroll’s etchant (1 mL HF + 4 mL HNO₃ + 100 mL distilled water)—were observed by optical microscopy (BX-53 M, Olympus, Japan). EBSD analysis was conducted using a scanning electron microscope (JSM-7900F, JEOL, Japan) in combination with an EBSD detector (C-Nano, Oxford Instruments, UK) to analyze the lath boundaries, phase distributions, and local misorientation distributions of the additively manufactured materials. Fractographic analyses of tensile-tested samples were conducted by coating them with Pt, using a sputter coater (208HR, Cressington, UK) to enhance their conductivity, and observing the samples by SEM.

3 Results

Figure 3 shows the optical micrographs of the Ti64 samples. The optical micrographs perpendicular to the building direction imply the Ti64-1 and Ti64-2 samples exhibit a lack of fusion owing to their low LEDs. The incidence and size of the voids resulting from a lack of fusion decrease

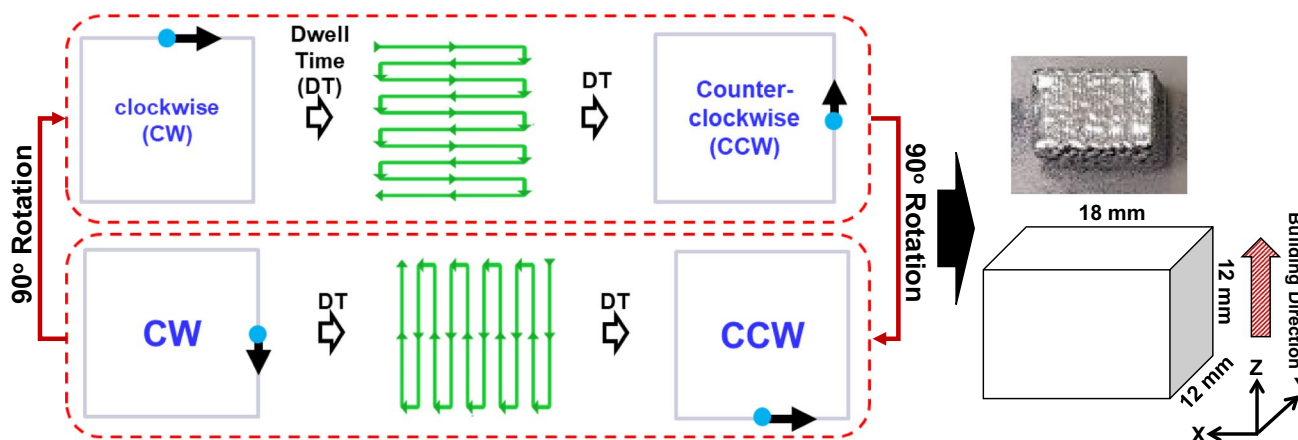


Fig. 2 Schematic of scan strategy and specimen dimensions of Ti64 samples

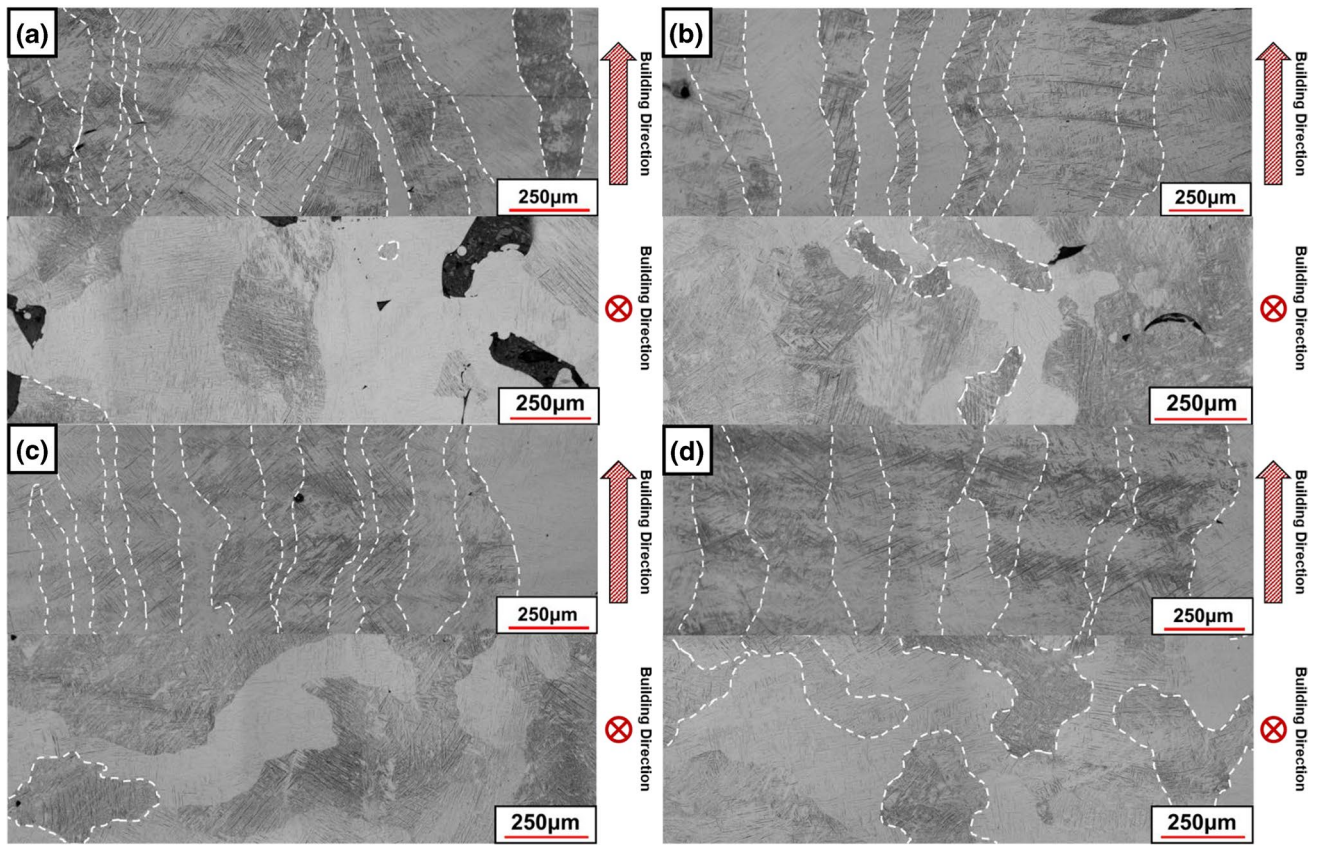


Fig. 3 Optical micrographs of the Ti64 samples: **a** Ti64-1, **b** Ti64-2, **c** Ti64-3, and **d** Ti64-4

with increasing LED, which implies that a LED of at least 12.7 J/mm is required to maximize the density of the Ti64 alloy. Higher LEDs lead to higher molten pool temperatures during laser-based AM [31]; as a result, the prior- β grain width after DED increases with the increasing LED. The optical micrograph along the building direction in Fig. 3 shows that the Ti64-1 and Ti64-4 samples contain relatively narrow ($99.35 \mu\text{m}$) and wide ($197.85 \mu\text{m}$) prior- β grains, respectively, indicating that the prior- β grain width indeed increases with increasing LED. The repeated heat exposure and thermal gradient that forms in the opposite direction to

the building direction during high-energy laser scanning, produce the columnar-shaped prior- β grains [17–19]. The high solidification rate of the DED process is sufficient to induce the complete formation of metastable α' martensite. The optical micrographs show that acicular α' martensite structures nucleate at prior- β grain boundaries and grow within the columnar prior- β grains. The EBSD inverse pole figure maps of the Ti64 samples (Fig. 4) show that acicular α' martensite structures develop hierarchically in prior- β grains. The average widths of the acicular α' martensite crystals in the Ti64-1, Ti64-2, Ti64-3, and Ti64-4 samples

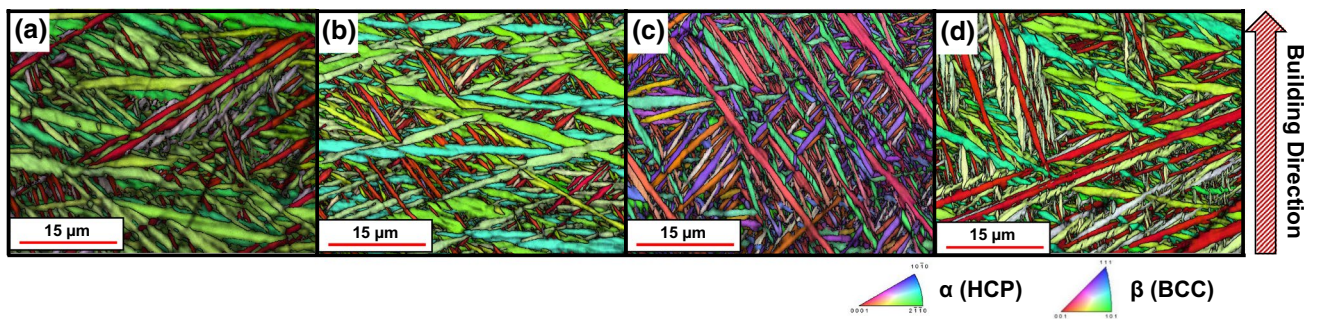


Fig. 4 EBSD inverse pole figure maps of the Ti64 alloy: **a** Ti64-1, **b** Ti64-2, **c** Ti64-3, and **d** Ti64-4

are 0.73 (± 0.43), 0.71 (± 0.41), 0.75 (± 0.45), and 0.82 (± 0.51) μm , respectively. Because the average lath widths are within the deviation, the average acicular α' martensite width of the Ti64 sample does not depend on the laser power.

To investigate the role of the microstructure in determining the mechanical properties of the Ti64 specimens, microhardness measurements and tensile tests were conducted. Figure 5 shows the relative density and microhardness of the Ti64 specimens as functions of LED. The relative densities of the Ti64 alloy can be correlated with the optical micrographs in Fig. 3, which show that the incidence and size of voids resulting from a lack of fusion decrease with increasing LED. Owing to the limited fusion achieved by its relatively low LED, the relative density of the Ti64-1 sample (0.925) is lower than those of other samples processed under higher LED conditions; relative density saturation is observed in the Ti64-2, Ti64-3, and Ti64-4 samples. A lack of fusion in additively manufactured parts impairs the mechanical properties of these parts, evidenced by the microhardness measurement results of the Ti64 samples shown in Fig. 5b. Interestingly, the microhardness of the Ti64 samples initially increases with increasing LED up to 12.7 J/mm (Ti64-2), but decreases when the LED exceeds 12.7 J/mm. To elucidate the plastic deformation behavior of the bulk materials, uniaxial tensile tests were conducted. Figure 6a presents the engineering stress–strain curves of the

Ti64 samples with a tensile strength and fracture strain of 1100–1200 MPa and 0.05–0.10, respectively. The mechanical properties of the Ti64 alloy depend on the LED during DED, Fig. 6b summarizes the strength and strain changes of the Ti64 samples with increasing LED. Similar to the microhardness measurement results in Fig. 5b, the Ti64-2 sample achieves the highest yield strength and tensile strength of the samples. Meanwhile, the tensile strain of the Ti64 samples increases with increasing LED up to 0.091 in the Ti64-3 sample before decreasing to 0.061 in the Ti64-4 sample.

SEM fractographs of the tensile-tested samples were obtained to correlate the fracture behavior with the tensile test results, as shown in Fig. 7. Because the extent of fusion and prior- β grain sizes of the Ti64 samples vary with changing LED, so do their fracture surfaces. Both seams (Fig. 7a-1) and voids, owing to incomplete fusion, (Fig. 7a-2) are observed on the fracture surface of the Ti64-1 sample in Fig. 7a, which serve as crack nucleation sites during tensile deformation. Although micro-dimples (Fig. 7a-3) are observed in the matrix of the Ti64-1 sample, crack nucleation from seams and voids—owing to a lack of fusion—dominates the fracture behavior of the sample and limits both its strength and ductility, as shown in Fig. 6. The fracture surface of the Ti64-2 sample in Fig. 7b shows regions that indicate the occurrence of dimple fracturing (Fig. 7b-2 and 3) and void coalescence (Fig. 7b-1) Such fracture behavior is consistent

Fig. 5 a Relative density and b microhardness as functions of LED of the Ti64-1, Ti64-2, Ti64-3, and Ti64-4 samples

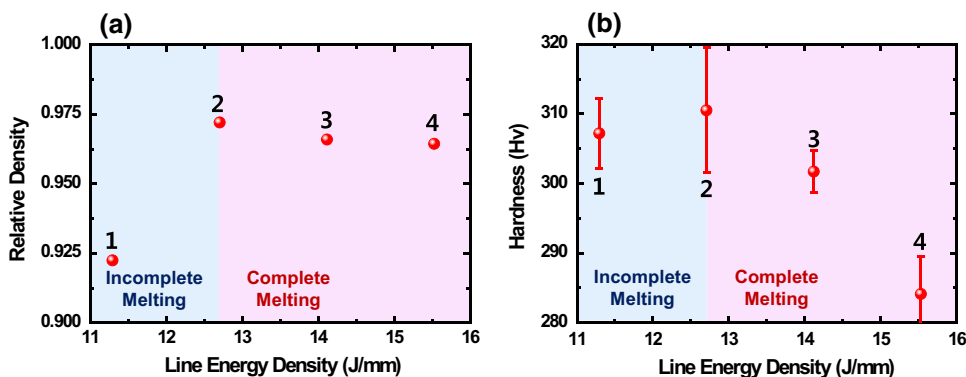
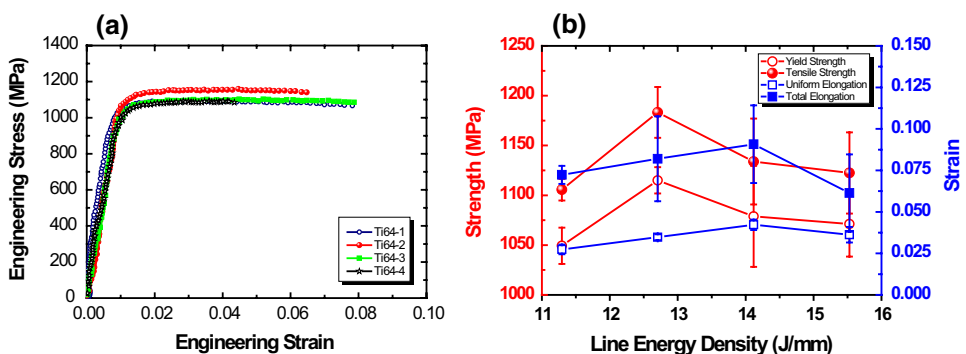


Fig. 6 a Engineering stress–strain curves of the Ti64-1, Ti64-2, Ti64-3, and Ti64-4 samples and their b strength and strain as functions of LED



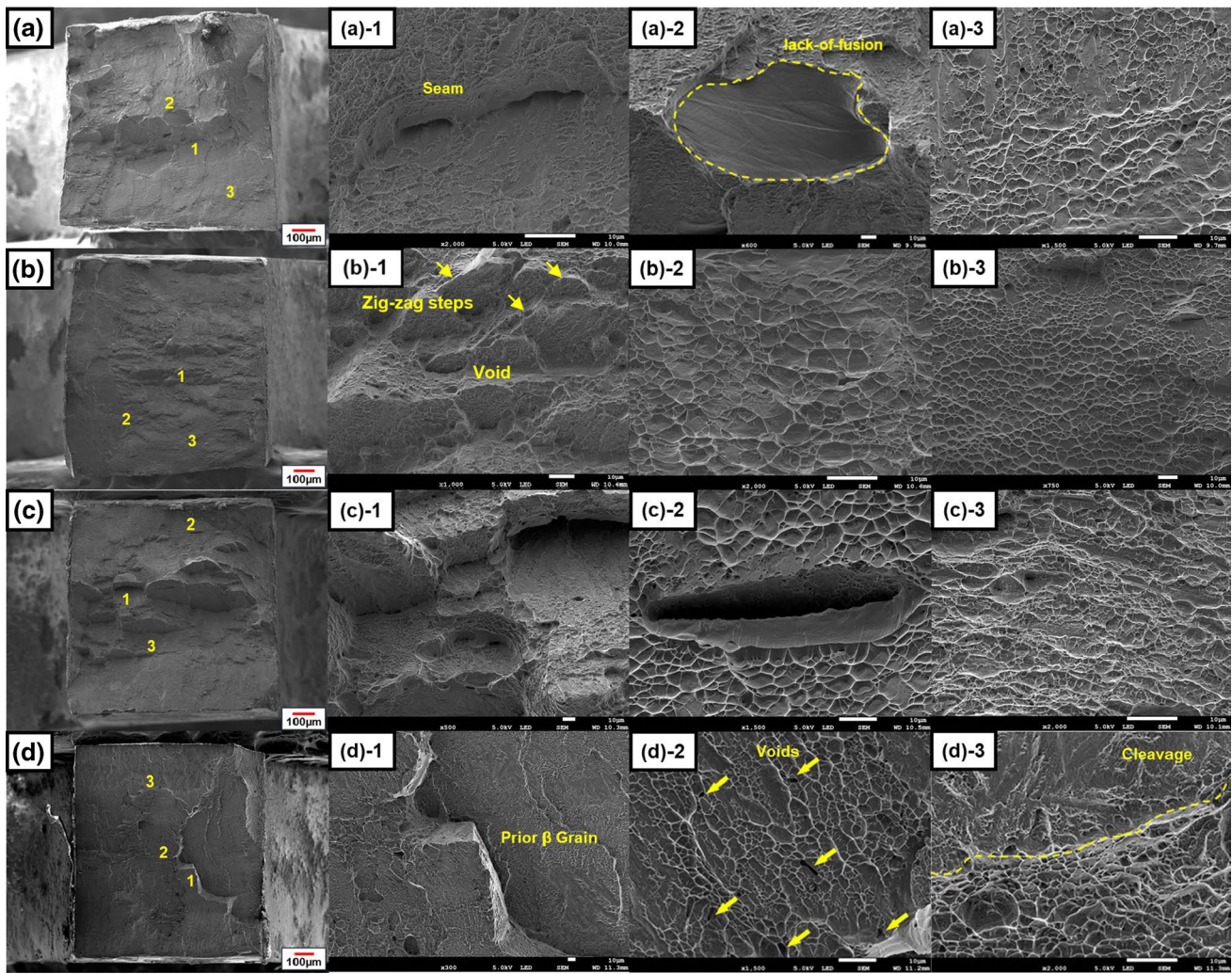


Fig. 7 SEM micrographs of the fracture surfaces of **a** Ti64-1, **b** Ti64-2, **c** Ti64-3, and **d** Ti64-4 samples

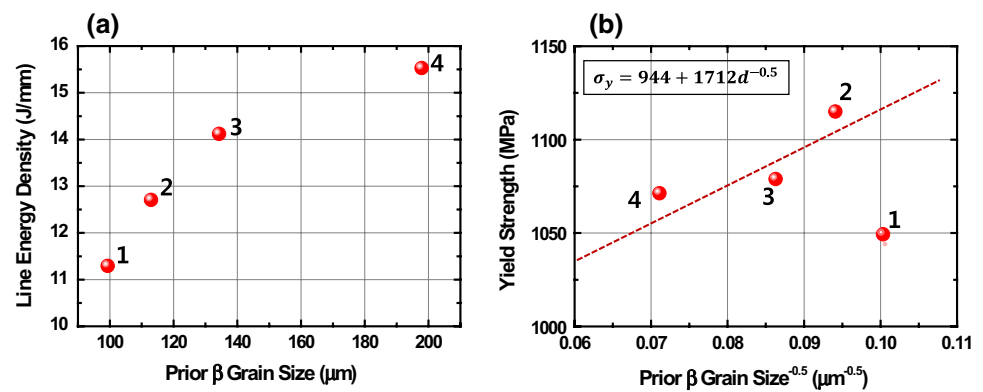
with that of dense, additively manufactured Ti64 alloy; ductile micro-voids nucleate on the lath martensite that merge with increasing plastic strain [32]. Moreover, zig-zag crack propagation in the Ti64-2 sample absorbs a significant amount of fracture energy, resulting in its high tensile strength. Similar to the Ti64-2 sample, the Ti64-3 sample (Fig. 7c) displays both dimple fracture (Fig. 7c-3) and void coalescence regions (Fig. 7c-1 and 2), indicating that ductile fracturing occurs in both the Ti64-2 and Ti64-3 samples. However, the coarse prior- β grains in the Ti64-3 sample induce delamination at the center of the tensile specimen, which slightly reduces its strength. In the case of the Ti64-4 sample, localized deformation and crack nucleation occur at prior- β grains boundaries owing to their coarse grain size ($\sim 330 \mu\text{m}$), and intergranular fracture occurs along these boundaries (Fig. 7d-1) [33]. In addition, relatively coarse voids (Fig. 7d-2) and cleavage fractures (Fig. 7d-3) are observed, indicating the low

ductility of the Ti64-4 sample; however, voids resulting from a lack of fusion are not observed.

4 Discussion

The experimental results show that the processing parameters affect the microstructures of DED-processed Ti64 samples, and the evolution of their microstructure during DED can be correlated with their mechanical properties and fracture surfaces. In this study, the laser power of the DED processes was expressed/defined in terms of their LEDs, and the properties of the Ti64 samples were correlated with the corresponding LEDs. Figure 8a represents the prior- β grain width of the Ti64 samples with the increase of LEDs, and the prior- β grain width exponentially increases with the increase of LED. This result shows that if the LED is larger than 15 J/mm, the

Fig. 8 **a** The grain size of Ti64 samples with the increase of LED. **b** Yield strength vs. prior- β grain size relation implies the yield strength of the Ti64 samples follows the Hall–Petch relation while the Ti64-1 sample has a deviation due to the lack of fusion



prior- β grain width drastically increases, and such a grain growth will degrade the mechanical property based on the Hall–Petch relation. Indeed, the Hall–Petch relation plot in Fig. 8b proves the yield strength of Ti64 samples has a Hall–Petch relation with a prior- β grain width except the Ti64-1 sample. The deviation of Ti64-1 sample is linked with the lack of fusion as observed in the optical micrograph in Fig. 3a, and this lack of fusion act as crack initiation site that limits the strength of Ti64 sample.

Thus, the relationship between LED and properties of Ti64 samples can be summarized as follows: (i) At a low LED, the obtained Ti64-1 sample contains a large number of sizable voids resulting from a lack of fusion (Fig. 3a) that serve as crack nucleation sites to limit its strength. Because the lack of fusion is more critical to the strength of the Ti64-1 sample than the Hall–Petch hardening associated with its small prior- β grain size, it exhibits the lowest tensile strength of all the samples. Moreover, the crack nucleation sites, i.e., voids resulting from the lack of fusion, induce delamination, as observed in the fracture surface of the Ti64-1 sample, limiting its ductility. (ii) At a moderate LED, the obtained Ti64-2 sample exhibits a relatively low incidence of voids (resulting from a lack of fusion), and its columnar prior- β grain and martensite lath widths are similar to those of the Ti64-1 sample. The strength impairment associated with the lack of fusion is negligible at this LED; consequently, the Ti64-2 sample exhibits the highest tensile strength of the samples. The zigzag cracks and secondary cracks in the fracture surfaces of the Ti64-2 and Ti64-3 samples indicate that these samples can absorb significant fracture energy, leading to high tensile elongation, as shown in Fig. 6b. (iii) At a high LED (> 14.11 J/mm), the coarsened prior- β grains of the obtained Ti64-4 sample are unable to interrupt dislocation gliding, significantly impairing its strength. Moreover, its columnar prior- β grains are relatively wide at $197.85 \mu\text{m}$, which means that only three prior- β grains exist in the tiny tensile specimen. The limited number of grains in the tensile specimen induces not only plastic instability during tensile testing but also intergranular

fracture along the prior- β grain boundaries (see Fig. 7d-1); resulting in relatively low ductility.

Therefore, the laser power during DED significantly affect the mechanical properties of additively manufactured Ti64 alloy, and the correlation of the mechanical properties of obtained alloy with the corresponding LEDs facilitates the determination of the optimal processing parameters. In this study, the optimal LED of $12.5\text{--}14.0$ J/mm minimizes the lack of fusion and the width of columnar prior- β grains to maximize the strength and ductility of Ti64 alloy. Although these results clearly demonstrate the relationship between LED and the properties of additively manufactured Ti64 alloy, this work does not consider other general processing parameters such as particle size distribution [34], AM machine type, and calibration parameters [35, 36]. Therefore, the development of a material property database that records the properties of materials obtained under different conditions (e.g., AM machine type and powder particle size, hatch spacing, layer thickness) is required to derive a more general relationship between the DED processing parameters and the properties of resultant materials.

5 Conclusions

In this study, the effect of the microstructure of DED-processed Ti64 alloy on their mechanical properties was investigated. The following conclusions are drawn based on the evaluation of the mechanical properties and the microstructural characterization of Ti64 alloy prepared under different processing conditions:

- (1) A relatively high LED during the DED of a Ti64 alloy not only promotes fusion but also increases the widths of its martensite laths and prior- β grains. The prior- β grain width of the Ti64 alloy increases with increasing LED from $115 \mu\text{m}$ (Ti64-1) to $330 \mu\text{m}$ (Ti64-4).
- (2) Voids resulting from a lack of fusion act as crack nucleation sites during plastic deformation, impairing the

- mechanical properties of materials. The strength and ductility of the Ti64 samples increase with increasing LED up to 12.7 J/mm owing to a concomitant decrease in the number of voids resulting from a lack of fusion.
- (3) Coarse prior- β grains limit the strength of Ti64 alloy processed at a high LED owing to the Hall–Petch relationship and induce plastic deformation instability in a small tensile specimen. Accordingly, both the strength and ductility of the Ti64 samples decrease when the LED exceeds 14.11 J/mm.
 - (4) The LED-based approach is useful for determining the optimal processing parameters for the manufacture of high-performance materials. Because the properties of additively manufactured products are influenced by the type of AM machine, calibration, and initial powder conditions, results from various laser-based AM machines and powders need to be collected to derive a general LED–material property relationship.

Acknowledgements This work was supported by the National Research Foundation of Korea (NRF) grant funded by the Korea government (MSIT) (2020R1A4A3079417). This work was also supported by the National Research Foundation of Korea (NRF) grant funded by the Korea government (MSIP) (2018R1A5A6075959). It was further supported by the National Research Foundation of Korea (NRF) grant funded by the Korea government (MSIP) (NRF-2021R1A2C3006662). H.S.K. acknowledges the great support funded by Ministry of Trade, Industry and Energy of Korea (20000495).

Data availability The raw/processed data required to reproduce these findings cannot be shared at this time as the data also forms part of an ongoing study.

References

1. M. Peters, J. Hemptenmacher, J. Kumpfert, C. Leyens, Structure and properties of titanium and titanium alloys, in *Titanium and Titanium Alloys: Fundamentals and Applications*, ed. by C. Leyens, M. Peters (Wiley-VCH, Weinheim, 2003), pp. 1–36
2. M.J. Donachie, *Titanium: A Technical Guide*, 2nd edn. (ASM International, Materials Park, OH, 2000)
3. R.R. Boyer, *Mater. Sci. Eng. A* **213**, 103 (1996)
4. Z.M. Wang, E.O. Ezugwu, *J. Mater. Process. Tech.* **68**, 262 (1997)
5. G.M. Karthik, H.S. Kim, *Met. Mater. Int.* **27**, 1 (2021)
6. D. Herzog, V. Seyda, E. Wycisk, C. Elmmelmann, *Acta Mater.* **117**, 271 (2016)
7. W.E. Frazier, *J. Mater. Eng. Perform.* **23**, 1917 (2014)
8. C. Zhong, J. Liu, T. Zhao, T. Schoppovben, J. Fu, A. Gasser, J.H. Schleifenbaum, *Appl. Sci.* **10**, 764 (2020)
9. I. Gibson, D. Rosen, B. Strucker, Directed energy deposition processes, in *Additive Manufacturing Technologies* (Springer, New York, NY, 2015), pp. 245–268
10. S.-K. Rittinghaus, J. Schmelzer, M.W. Rackel, S. Hemes, A. Vogelphoth, U. Hecht, A. Weisheit, *Materials* **13**, 4392 (2020)
11. S. Tumuluri, P. Murugesan, R.K. Mishra, V.V. Subrahmanyam, *J. Fail. Anal. Prev.* **17**, 788 (2017)
12. T. Bhardwaj, M. Shukla, N.K. Prasad, C.P. Paul, K.S. Bindra, *Met. Mater. Int.* **26**, 1015 (2020)
13. D.-K. Kim, W. Woo, E.-Y. Kim, S.-H. Choi, *J. Alloy. Compd.* **774**, 896 (2019)
14. S.M.J. Razani, F. Berto, *Adv. Eng. Mater.* **21**, 1900220 (2019)
15. C.L.A. Leung, S. Marussi, R.C. Atwood, M. Towrie, P.J. Withers, P.D. Lee, *Nat. Commun.* **9**, 1355 (2018)
16. W. Hofmeister, M. Griffith, *JOM* **53**, 30 (2001)
17. M. Simonelli, Y.Y. Tse, C. Tuck, *Mater. Sci. Eng. A* **616**, 1 (2014)
18. J. Yang, H. Yu, J. Yin, M. Gao, Z. Wang, X. Zeng, *Mater. Design* **108**, 308 (2016)
19. I.-S. Kim, J.M. Oh, S.W. Lee, J.-T. Yeom, J.-K. Hong, C.H. Park, T. Lee, *J. Mater. Res. Technol.* **12**, 304 (2021)
20. R.M. Mahamood, E.T. Akinlabi, M. Shukla, S. Pityana, *J. Manuf. Sci. Eng.* **135**, 064502 (2013)
21. S. Sahoo, K. Chou, *Addit. Manuf.* **9**, 14 (2016)
22. R.M. Mahamood, E.T. Akinlabi, S.A. Akinlabi, *Lasers Manuf. Mater. Process.* **2**, 43 (2014)
23. R.M. Mahamood, E.T. Akinlabi, *Int. J. Adv. Manuf. Technol.* **91**, 2419 (2017)
24. X. Wu, J. Liang, J. Mei, C. Mitchell, P.S. Goodwin, W. Voice, *Mater. Design* **25**, 137 (2004)
25. X. Tan, Y. Kok, Y.J. Tan, M. Descoins, D. Mangelinck, S.B. Tor, K.F. Leong, C.K. Chua, *Acta Mater.* **97**, 1 (2015)
26. J. Lin, Y. Lv, Y. Liu, Z. Sun, K. Wang, Z. Li, Y. Wu, B. Xu, *J. Mech. Behav. Miomed.* **69**, 19 (2017)
27. D. Cheng, J. Zhang, T. Shi, G. Li, J. Shi, L. Lu, G. Fu, *Opt. Laser Technol.* **135**, 106640 (2021)
28. J. Li, H. Ren, C. Liu, S. Shang, *Materials* **12**, 1321 (2019)
29. M.H. Farshidianfar, F. Khodabakhshi, A. Khajepour, A.P. Gerlich, *Mater. Sci. Eng. A* **803**, 140483 (2021)
30. J.I. Yoon, J.G. Kim, J.M. Jung, D.J. Lee, H.J. Jeong, M. Shahbaz, S. Lee, H.S. Kim, *Korean J. Met. Mater.* **54**, 231 (2016)
31. Z. Xiang, M. Yin, G. Dong, X. Mei, G. Yin, *Results Phys.* **9**, 939 (2018)
32. A. Moridi, A.G. Demir, L. Caprio, A.J. Hart, B. Previtali, B.M. Colosimo, *Mater. Sci. Eng. A* **768**, 138456 (2019)
33. J.W. Foltz, B. Welk, P.C. Collins, H.L. Fraser, J.C. Williams, *Metall. Mater. Trans. A* **42**, 645 (2011)
34. Y. Kakinuma, M. Mori, Y. Oda, T. Mori, M. Kashihara, A. Hansel, M. Fujishima, *CIRP Ann.* **65**, 209 (2016)
35. M. Seifi, M. Gorelik, J. Waller, N. Hrabe, N. Shamsaei, S. Daniewicz, J.J. Lewandowski, *JOM* **69**, 439 (2017)
36. B. Brenken, E. Barocio, A. Favaloro, V. Kunc, R.B. Pipes, *Addit. Manuf.* **25**, 218 (2019)

Publisher's Note Springer Nature remains neutral with regard to jurisdictional claims in published maps and institutional affiliations.